

See discussions, stats, and author profiles for this publication at: <https://www.researchgate.net/publication/342348229>

# Time-resolved characterization of ultrafast electrons in intense laser and metallic-dielectric target interaction

Preprint · June 2020

CITATIONS

0

READS

54

7 authors, including:



**Mario Galletti**

University of Rome Tor Vergata

115 PUBLICATIONS 474 CITATIONS

SEE PROFILE



**Fabrizio Bisesto**

Leonardo SpA

85 PUBLICATIONS 1,077 CITATIONS

SEE PROFILE



**Maria Pia Anania**

INFN - Istituto Nazionale di Fisica Nucleare

177 PUBLICATIONS 2,706 CITATIONS

SEE PROFILE



**Massimo Ferrario**

INFN - Istituto Nazionale di Fisica Nucleare

617 PUBLICATIONS 8,307 CITATIONS

SEE PROFILE

Some of the authors of this publication are also working on these related projects:



L2I laser development [View project](#)



CompactLight XLS Project [View project](#)

# Time-resolved characterization of ultrafast electrons in intense laser and metallic-dielectric target interaction.

M. GALLETTI<sup>1,2,3,\*</sup>, F.G. BISESTO<sup>1</sup>, M.P. ANANIA<sup>1</sup>, M. FERRARIO<sup>1</sup>, R. POMPILI<sup>1</sup>, A. POYÉ<sup>4</sup>, AND A. ZIGLER<sup>1,5</sup>

<sup>1</sup>INFN Laboratori Nazionali di Frascati, Via Enrico Fermi 40, 00044 Frascati, Italy

<sup>2</sup>GoLP/Instituto de Plasmas e Fusao Nuclear, Instituto Superior Tecnico, Universidade de Lisboa, 1049-001 Lisboa, Portugal

<sup>3</sup>Central Laser Facility, Science and Technology Facilities Council, Rutherford Appleton Laboratory, Harwell Science and Innovation Campus, Didcot, UK

<sup>4</sup>Laboratory PIIIM, University Aix-Marseille - CNRS, Avenue Escadrille Normandie-Niemen, 13397 Marseille, France

<sup>5</sup>Racah Institute of Physics, Hebrew University, 91904 Jerusalem, Israel

\*Corresponding author:mario.galleggi@stfc.ac.uk

Compiled June 17, 2020

**High intensity ultrashort laser pulses interacting with thin solid targets are able to produce energetic ion beams by means of extremely large accelerating fields set by the energetic ejected electrons. The characterization of such electrons is thus important in view of a complete understanding of the acceleration process. Here, we present a complete temporal-resolved characterization of the fastest escaping hot electron component for different target material and thickness, using a temporal diagnostics based on Electro-Optical Sampling with 100 fs temporal resolution. Experimental evidence of scaling laws for ultrafast electron beam parameters have been retrieved with respect to the impinging laser energy (0.4 - 4 J range) and to the target material, and an empirical law determining the beam parameters as a function of the target thickness is presented.** © 2020 Optical Society of America

<http://dx.doi.org/10.1364/ao.XX.XXXXXX>

High-power, ultrafast lasers interacting with solid matter are able to produce electron, proton and heavier ion beams over a wide range of energy [1, 2], opening the way for new experiments in different areas like nuclear fusion science, laser-based acceleration [3–5] and medical research [6]. Ion acceleration from thin targets, in particular, has been extensively investigated: the huge accelerating gradient (of the order of TV/m) produced by such interactions can provide ion and proton beams of several tens of MeV and nC charge [7–9]. According to current theoretical models, valid for laser-target experiments working in relativistic regime [10], the picture of the process is the following: the ultrashort laser pulse impinges on the front target surface, forming plasma and directly accelerates energetic electrons that originate various effects such as intense X-ray emission, ion acceleration, and giant electromagnetic pulses. A component of the energetic electrons, (hereinafter called *hot* electrons), after escaping from the target and leaving it positively charged [11], sets on it an electrostatic potential. The latter is capable to ionize

and accelerate, along the direction normal to the target, surface ions and protons [12]. This process is called Target Normal Sheath Acceleration [13] (TNSA). So far in TNSA experiments, only indirect or time-integrated measurements of the escaped electrons have been shown [14–16]. Recently, we have started a detailed time-resolved study of the release mechanism [17–21] by employing a diagnostic based on Electro-Optical Sampling (EOS), widely used in accelerator facilities [22, 23]. In this *Letter*, we report direct temporally-resolved measurements of *ultrafast* (*uf*) electron component ejected from a solid target after the interaction with an ultrashort high-intensity laser pulse, varying its energy in the  $\sim 0.4 - 4$  J range. This population is compound by the most energetic hot electrons, i.e. the first forerunners escaping the target while the development of the potential barrier. It plays a major role in subsequent processes, like the ultrafast dynamics of the electrostatic potential. As highlighted in literature [24], the dynamics of such particles does not follow the usual hot electron escaping models [10, 25], showing a free ballistic dynamics that occurs before any collisions and during the potential barrier raise. For this purpose, EOS is used to provide snapshots of the escaping fast electrons with resolution of the order of 100 fs. The obtained experimental data show, for the first time, the comparison of the scaling of the ultrafast electrons charge and duration as a function of the laser intensity for different materials, stainless steel and sapphire (sapphire windows [26]), and thicknesses. The results have been compared with well-established theoretical models [10], showing an excellent agreement. Furthermore, for the first time, an empirical law determining the electron beam parameters as a function of the target thickness, maintaining a constant laser energy, is presented. The experiment has been carried out at SPARC\_LAB Test Facility [27] with the setup shown in Fig. 1. Here the 150 TW Ti:Sa FLAME laser system [28] delivers 25 fs (FWHM) pulses with up to 4 J (on target) at 800 nm central wavelength and 10 Hz repetition rate. The system consists of a CPA chain providing more than 6 J at the final cryo-amplifier output. After optical compression, the laser beam is focused by an  $f/10$  off-axis parabolic mirror (focal length  $f = 1$  m), reaching a final spot size of 15  $\mu\text{m}$  ( $1/e^2$  radius). Considering 70% as total energy transport

efficiency, a peak intensity of  $2 \times 10^{19} \text{ W/cm}^2$  (corresponding to a normalized laser intensity  $a_0 > 3$ ) is achieved on the target, hosted in a high vacuum environment ( $10^{-6}$  mbar). Furthermore, the temporal contrast is  $10^{-6}$  at ps-level and below  $10^{-9}$  at ns-scale. The high-intensity ultrashort FLAME laser is focused

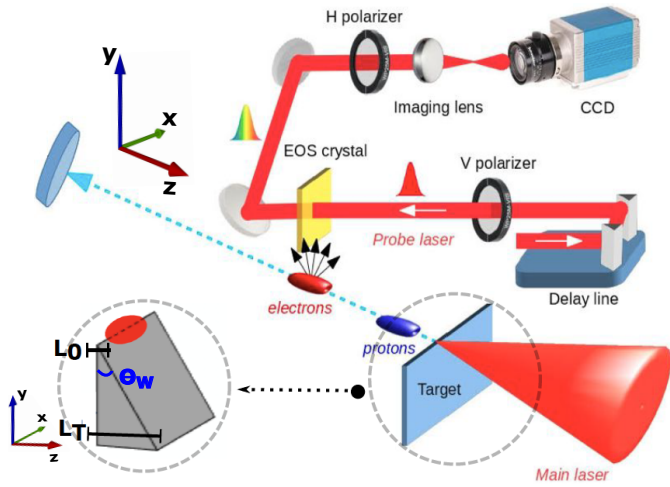


**Fig. 1.** Setup of the experiment. The FLAME laser is focused on a stainless steel/sapphire target ejecting electrons. The EOS system, based on a ZnTe crystal placed 1 mm downstream the target, measures the electric field and temporal profile of the emitted electrons by means of a probe laser directly split from the main one. **The z-axis corresponds to the propagation axis perpendicular to the target.** Inset: The metallic target sketch is shown.

onto a  $5 \mu\text{m}$  thick stainless steel wedged target or a  $400 \mu\text{m}$  thick sapphire target (uncoated; surface quality: 80-50 S-D; flatness:  $< \lambda/4$ ; LIDT:  $1 \text{ J/cm}^2$  at  $1064 \text{ nm}$ ,  $10 \text{ ns}$ ; resistivity:  $10^{16} \Omega\text{-cm}$  at  $25^\circ$  to  $10^6 \Omega\text{-cm}$  at  $1000^\circ$ ). The fast electrons, produced by the laser-target interaction and escaping from it, are detected by the EOS diagnostics consisting of a  $500 \mu\text{m}$  thick ZnTe crystal, located  $1 \text{ mm}$  downstream the target. The moving electron beam propagates  $1 \text{ mm}$  below the EOS crystal, as shown in Fig. 1. The EOS relies on a  $30 \text{ fs}$  probe laser, directly split from the main one, ensuring a jitter-free synchronization, impinging into the crystal with  $28^\circ$  incidence angle providing an effective time-window of  $\approx 10 \text{ ps}$ , as dictated by the spatial decoding technique[23]. The EOS setup is completed by a lens installed downstream the crystal, used to image the laser impinging the crystal on the CCD camera where the EOS signals are actually recorded. The temporal overlap of the main and probe lasers in correspondence of the EOS crystal is obtained by finding the auto-correlation signal with an  $\alpha$ -cut BBO crystal installed on the ZnTe holder. For this purpose a  $3 \text{ fs}$  resolution delay-line (Fig. 1) on the probe path is employed. Once such a reference time is determined, the probe delay-line is moved to ensure the synchronization with the emitted electrons and in turn to produce the EOS signal. The electric field of the ultrafast electrons is thus spatially imprinted along the transverse profile of the temporally synchronized probe laser. The EOS spatial encoding process is presented in [19, 20, 29, 30]. It shows the currently implemented geometry of the EOS setup, i.e. electrons travelling below and perpendicularly to the crystal while the probe laser propagates with an angle from right side to the left side. The local birefringence induced by the beam E-field and the probe laser overlap temporally and spatially. The use

of the EOS diagnostic is fundamental to select and characterize only the fast component of the emitted electrons while the hot one is disregarded due to its slowness to reach the EOS crystal location. Figure 2 shows a typical EOS snapshot recorded after the interaction of the FLAME laser with the wedged target (left) and a dielectric target (right). The lack of uniformity in the experimental signals is mainly due to inhomogeneities both on the ZnTe crystal surface and on the transverse profile of the probe laser. The total charge ( $Q_{uf}$ ), the electric field ( $\Sigma_{uf}$ ) and duration ( $\tau_{uf}$ ) of the emitted electrons are then retrieved from the signal amplitude and width [19], respectively. The electron parameters

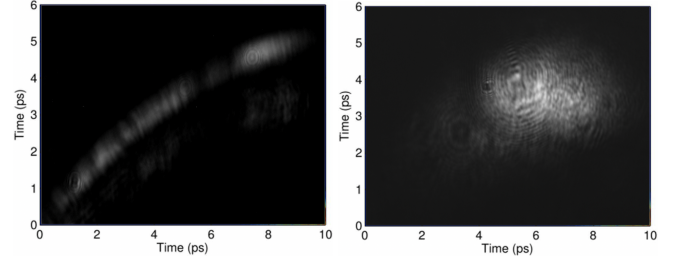


**Fig. 2.** Detected EOS signal. Adopting  $\sim 4 \text{ J}$  laser energy, an electron beam with a  $\tau_{uf} \sim 500 \text{ fs}$  for the metallic target (L), while  $\tau_{uf} \sim 1.5 \text{ ps}$  for the dielectric one (R) is observed.

value, relative to the total charge and the electric field peak in correspondence of the EOS crystal, have been acquired for different laser energy on target, as shown in Fig. 3. The vertical error bars represent the standard deviation calculated for  $N = 10$  shots for each point. For the laser energy, the measured r.m.s. value is used. From here, it is noticeable that in TNSA regime the extracted charge increases for higher laser energy delivered on target; in turn, an increase of the induced electric field is shown, according to the well-known Coulomb law. The experimental

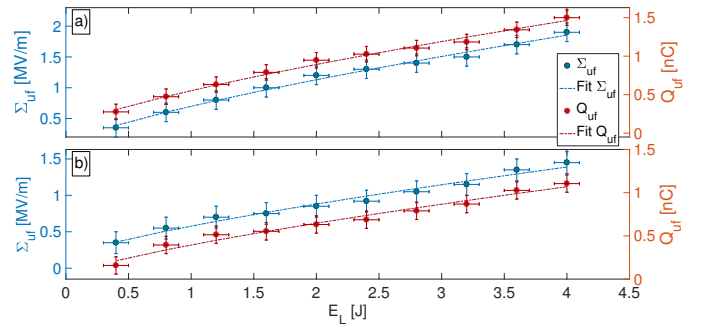


**Fig. 3.** Experimental scaling relative to the tip,  $L_0 = 5 \mu\text{m}$ , of wedged-metallic target (a) and to the  $400 \mu\text{m}$  dielectric target (b). (Blue circles) Peak E-field and (Red circles) the charge associated with the ultrafast electron bunches as function of the laser energy.

data fits, blue and red dashed lines in Fig. 3, were performed adopting two power functions, namely  $\Sigma_{uf} = \alpha * E_L^{n_1} + \delta$  and  $Q_{uf} = \beta * E_L^{n_2} + \gamma$  with  $\alpha, \beta, \gamma, \delta, n_1$  and  $n_2$  used as free parameters. From experimental data, we found for the wedged-metallic target  $\Sigma_{uf} = (0.63 \pm 0.04) E_L^{(0.746 \pm 0.02)} + (0.07 \pm 0.04)$  and  $Q_{uf} = (0.50 \pm 0.03) E_L^{(0.746 \pm 0.02)} + (0.06 \pm 0.04)$  while for the dielectric target  $\Sigma_{uf} = (0.44 \pm 0.04) E_L^{(0.748 \pm 0.02)} + (0.11 \pm 0.04)$  and  $Q_{uf} = (0.37 \pm 0.04) E_L^{(0.749 \pm 0.02)} + (0.03 \pm 0.02)$ . To support

our experimental results, an analytic scaling law was also retrieved from some well established theories found in literature [10, 31–33]. Indeed, considering the laser energy ( $E_L$ ) to hot electrons conversion efficiency [10]  $\eta = 1.75 * 10^{-4} * I_L^{1/4}$ , where  $I_L = E_L / (\tau_L * S_L)$  is the laser intensity characterized by  $\tau_L$  and  $S_L$  respectively the laser duration and spot extension, it is possible to retrieve their number as  $N_{hot} = \eta E_L / E_{hot}$  where  $E_{hot}$  is the energy of the hot electrons [31, 32], highly dependent on the laser energy, defined as  $E_{hot} = E_0 * \max[0.47 * a_0^{2/3}, \sqrt{1 + a_0^2} - 1]$ . Here,  $E_0$  is the electron energy at rest and  $a_0 = 0.85 * 10^{-9} * \lambda_L [\mu m] * I_L^{1/2}$  the normalized laser potential, with  $\lambda_L$  the laser central wavelength. The ejected electrons, crossing the solid-vacuum boundary, induce a positive charge on the rear surface, leading to a potential according to Poisson's law. Meanwhile this potential acts as a driver for the ions that overcome the bonding force and start to be accelerated reaching energies up to several tens of MeV; for the electrons it acts as a potential barrier near the target. In turn, it confines the majority of the ejected low energetic electrons in the target vicinity. However, while the potential is setting up, a fraction of hot electrons, i.e.  $N_{uf} = \delta * N_{hot}$  with  $\delta \sim 1\%$  [17, 18], can still leave the target and be measured by the EOS diagnostic. Since  $E_{hot} \propto a_0$  in our intensity range, we analytically retrieve that  $N_{uf} \propto \Sigma_{uf} \propto Q_{uf} \propto E_L^{3/4}$ , showing an excellent agreement with the experimental data. Moreover, for the wedged metallic target, it was possible to realize a scan of the target thickness thanks to its shape (wedge angle  $\Theta_W \sim 17^\circ \pm 3^\circ$ ). As shown in Fig.4, a linear behaviour is found:

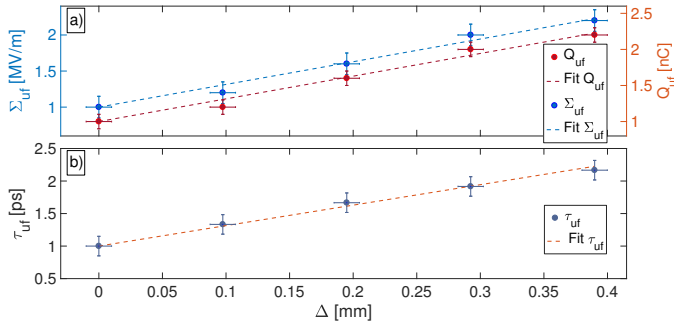


**Fig. 4.** Thickness scan performed with  $E_L = 4$  J. a) (Blue circles) Peak E-field, (Red circles) the charge and b) temporal length (blue circles) associated with the electron bunches as function of the increment in target thickness  $\Delta$ . The thickness error is considered as the slit resolution.

increasing the thickness, more electrons are being extracted, thus higher charge and consequently higher E-field are detected. We retrieved for the first time an empirical law, as shown in Fig.4 for 4 J laser energy. For the sake of completeness, we also verified this behaviour for our range of intensities ( $0.4 < E_L < 4$  J), not shown here. The experimental data fits, blue and red dashed lines in Fig.4,a, were performed adopting two linear functions, namely  $\frac{\Sigma_{uf}}{\Sigma_0} = (1 + \Omega\Delta)$  and  $\frac{Q_{uf}}{Q_0} = (1 + \Omega_1\Delta)$  where  $\Delta = L_T - L_0$  where  $L_T$  is the target thickness and  $L_0 = 5\mu m$  the tip thickness;  $\Omega$  and  $\Omega_1$  are free parameters while  $\Sigma_0$  and  $Q_0$  are retrieved from the data at maximum energy for  $\Delta = 0$  meaning  $L_T = L_0 = 5\mu m$ , as in Fig.3,a. The value of the coefficients  $\Omega$  and  $\Omega_1$  is  $3.15 \pm 0.35$ . This linear scaling laws are in agreement with the one implemented in the developed simplified scalar model, Electron Ballistic-propagation Code (EBC) [24], able to

complete the well-known ChoCoLaTII simulation code [11, 34]. The ultrafast electron charge, with a linear dependence on the target thickness, is given by

$$Q_{uf} \simeq L_T \times \int_{V_p}^{\infty} \eta \frac{eE_L \exp(-\varepsilon/E_{hot})}{\tau_L} \times \left( \frac{1}{v(V_p)} - \frac{1}{v(\varepsilon)} \right) d\varepsilon$$

where  $e$  is the electron elementary charge,  $V_p$  the potential barrier [24, 35],  $\varepsilon$  is the electron energy and  $v(\varepsilon)$  is the electron speed. Furthermore, the EOS diagnostic allows also to mea-

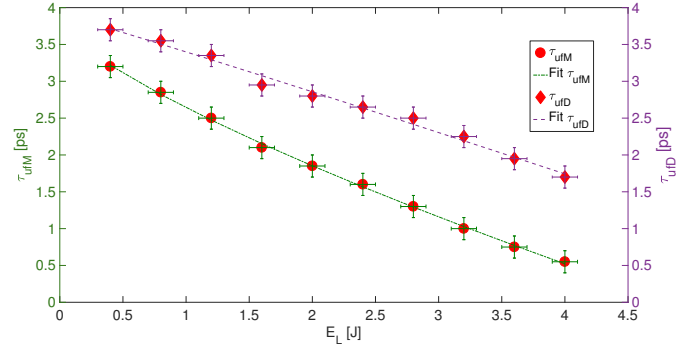


**Fig. 5.** Electron temporal length (Red circles and diamonds) as function of the laser energy. A power law (Green dashed line) and a linear one (Purple dashed line) for the wedged-metallic and dielectric targets, respectively, are found.

sure fast electron beam temporal duration. The retrieved beam temporal length, as a function of laser energy, is reported in Fig. 5, showing different behaviours for the two adopted material. Indeed, the experimental data were compared with respect to a power function. In detail, it turns out  $\tau_{ufM} = \chi * E_L^\zeta + \nu$  with  $\zeta = 0.7 \pm 0.1$ ,  $\chi = -1.3 \pm 0.4$  and  $\nu = 3.9 \pm 0.4$  (green dashed line in Fig.5). On the other hand, for the dielectric material (purple dashed line in Fig.5) it turns out  $\tau_{ufD} = \chi * E_L^\zeta + \nu$  with  $\zeta = 1 \pm 0.15$ ,  $\chi = -0.5 \pm 0.15$  and  $\nu = 3.9 \pm 0.3$ . In the case of the metallic target, the electron bunch temporal length shortens increasing the laser energy (about six times), more respect to the dielectric target (about two times). In detail, two scenarios are verified: at high laser intensity, relativistic electrons are ejected with small velocity spread ( $\beta \approx 1$ ), resulting in a shorter bunch, while a strong decelerating potential acts as a high-velocity-pass filter; on the other side, at lower laser energy, the electrons are less relativistic ( $\beta < 1$ ) and the beam temporal elongation due to the velocity spread is stronger, furthermore increased by an albeit weaker potential, still acting as a velocity filtering. Even for the beam temporal duration, a target thickness scan was performed for the wedged metallic at maximum laser energy (Fig.4,b). From the experimental data, we observed a linear behaviour: increasing the thickness of about 400  $\mu m$ , the temporal length is stretched by a factor  $\sim 2$ . As previously shown in Fig.4,a, higher is the charge, stronger is the stretching effect (namely the space charge effect) on the electron bunch. The experimental data fits, blue dashed lines in Fig.4,b, were performed adopting a linear functions, namely  $\frac{\tau_{uf}}{\tau_0} = (1 + \Omega_2\Delta)$  with  $\Omega_2$  used as free parameter while  $\tau_0$  is retrieved from at maximum energy for  $\Delta = 0$  meaning  $L_T = L_0 = 5\mu m$ , as in Fig.5,a. The value of the coefficients  $\Omega_2$  is  $3.1 \pm 0.2$ , coinciding with the empirical law regarding the beam charge (and consequently the E-field). This result highlights that the temporal length strongly depends on the charge of the bunch; the space

charge force ( $\propto Q/\gamma^2$ ) can be the dominant effect during the propagation for relatively low energy electron, meaning relatively low laser energy, as already pointed out in [24]. We have presented direct temporally-resolved sub-picosecond resolution measurements of the *ultrafast* electron beams ejected from solid targets performed by varying the laser energy impinging onto the target. In particular, the total emitted charge and the bunch temporal length have been estimated by means of a numerical code [17–19] and analytic calculation were performed to validate the scaling law experimentally retrieved. Our experimental data show beams with charge of approximately  $\sim 1.5$  nC (1.1 nC) and temporal length of  $\sim 0.5$  ps (1.5 ps) escaping from target and traveling up to the EOS crystal for the maximum FLAME energy for the wedged metallic (dielectric) target; on the other hand, for the minimum energy available (corresponding to the 10% of the maximum) electron bunches with charge of approximately  $\sim 0.3$  nC (0.2 nC) and temporal length of  $\sim 2.7$  ps (3.7 ps) are measured. In turn, for our experimental parameters, the metallic wedged targets yield shorter high charged electron beams. A possible explanation is that the charge spreads much faster on the the surface of metallic target than the dielectric one so we are losing slower electrons sideways. Because of the conductivity and high laser-induced damage threshold, allowing minimization of contrast issues, transparent conductive oxides such as  $\text{Ga}_2\text{O}_3$ [36] or semiconductors[37] can be adopted to potentially lead to shorter bunches. We found out the beam charge and the E-field scale as  $E_L^{3/4}$  and the beam temporal length scales almost linearly with the laser energy in both cases, showing an excellent agreement with the well known theoretical model[10]. Furthermore, an empirical law describing the electron beam parameters as a function of the target thickness, is retrieved. In turn, a thicker metallic target allows to retrieve higher charged but longer beams. A linear behaviour is highlighted for all the electron beam parameters. Finally, we showed the EOS diagnostic represents a suitable tool in order to probe the temporal evolution of the ultrafast electron component influenced by the induced potential barrier near the target surface. Furthermore, because of the electrostatic potential successively establishes the following protons and heavier ions acceleration, the EOS diagnostics can represent a powerful tool to have a deeper understanding of the entire TNSA acceleration process.

**Disclosures.** The authors declare no conflicts of interest.

## REFERENCES

- B. A. Remington, D. Arnett, R. Paul *et al.*, *Science* **284**, 1488 (1999).
- T. Bartal, M. E. Foord, C. Bellei, M. H. Key, K. A. Flippo, S. A. Gaillard, D. T. Offermann, P. K. Patel *et al.*, *Nat. Phys.* **8**, 139 (2012).
- D. Kaganovich, D. Gordon, and A. Ting, *Phys. Rev. Lett.* **100**, 215002 (2008).
- M. Kozak, J. McNeur, K. Leedle *et al.*, *Nat. Comm.* **8**, 14342 (2017).
- J. McNeur, M. Kozak, N. Schönerberger, K. J. Leedle, H. Deng, A. Ceballos, H. Hoogland, A. Ruehl, I. Hartl, R. Holzwarth, O. Solgaard, J. S. Harris, R. L. Byer, and P. Hommelhoff, *Optica* **5**, 687 (2018).
- K. W. Ledingham, P. R. Bolton, N. Shikazono, and C.-M. C. Ma, *Appl. Sci.* **4**, 402 (2014).
- E. Clark, K. Krushelnick, M. Zepf, F. Beg, M. Tatarakis, A. Machacek, M. Santala, I. Watts, P. Norreys, and A. Dangor, *Phys. Rev. Lett.* **85**, 1654 (2000).
- R. Snavely, M. Key, S. Hatchett, T. Cowan, M. Roth, T. Phillips, M. Stoyer, E. Henry, T. Sangster, M. Singh *et al.*, *Phys. Rev. Lett.* **85**, 2945 (2000).
- A. Mackinnon, Y. Sentoku, P. Patel, D. Price, S. Hatchett, M. Key, C. Andersen, R. Snavely, and R. Freeman, *Phys. Rev. Lett.* **88**, 215006 (2002).
- J. Dubois, F. Lubrano-Lavaderci, D. Raffestin, J. Ribolzi, J. Gazave, A. C. La Fontaine, E. d'Humières, S. Hulin, P. Nicolaï, A. Poyé *et al.*, *Phys. Rev. E* **89**, 013102 (2014).
- A. Poyé, J. Dubois, F. Lubrano-Lavaderci, E. D'Humières, M. Bardon, S. Hulin, M. Bailly-Grandvaux, J. Ribolzi, D. Raffestin, J. Santos *et al.*, *Phys. Rev. E* **92**, 043107 (2015).
- A. Macchi, M. Borghesi, and M. Passoni, *Rev. Mod. Phys.* **85**, 751 (2013).
- S. Wilks, A. Langdon, T. Cowan, M. Roth, M. Singh, S. Hatchett, M. Key, D. Pennington, A. MacKinnon, and R. Snavely, *Phys. Plasmas* **8**, 542 (2001).
- O. Jäckel, J. Polz, S. Pfoth, H. Schlenvoigt, H. Schwoerer, and M. Kaluza, *New J. Phys.* **12**, 103027 (2010).
- P. Nilson, J. Davies, W. Theobald, P. Jaanimagi, C. Mileham, R. Jungquist, C. Stoeckl, I. Begishev, A. Solodov, J. Myatt *et al.*, *Phys. Rev. Lett.* **108**, 085002 (2012).
- J. T. Morrison, S. Feister, K. D. Frische, D. R. Austin, G. K. Ngirmang, N. R. Murphy, C. Orban, E. A. Chowdhury, and W. Roquemore, *New J. Phys.* **20**, 022001 (2018).
- R. Pompili, M. Anania, F. Bisesto, M. Botton, M. Castellano, E. Chiadroni, A. Cianchi, A. Curcio, M. Ferrario, M. Galletti *et al.*, *Sci. Rep.* **6**, 35000 (2016).
- R. Pompili, M. Anania, F. Bisesto, M. Botton, E. Chiadroni, A. Cianchi, A. Curcio, M. Ferrario, M. Galletti *et al.*, *Sci. Rep.* **8**, 3243 (2018).
- R. Pompili, M. Anania, F. Bisesto, M. Botton, M. Castellano, E. Chiadroni, A. Cianchi, A. Curcio, M. Ferrario, M. Galletti *et al.*, *Opt. Express* **24**, 29512 (2016).
- F. Bisesto, M. P. Anania, M. Botton, E. Chiadroni, A. Cianchi, A. Curcio, M. Ferrario, M. Galletti *et al.*, *Quantum Beam Sci.* **1**, 13 (2017).
- F. Bisesto, M. Galletti, M. Anania, M. Ferrario, R. Pompili *et al.*, *High Power Laser Sci. Eng.* **7** (2019).
- B. Steffen, V. Arsov, G. Berden, W. Gillespie, S. Jamison, A. M. MacLeod, A. Van Der Meer, P. Phillips, H. Schlarb, B. Schmidt *et al.*, *Phys. Rev. Special Top. Beams* **12**, 032802 (2009).
- A. L. Cavalieri, D. Fritz, S. Lee, P. Bucksbaum, D. Reis, J. Rudati, D. Mills, P. Fuoss, G. Stephenson, C. Kao *et al.*, *Phys. Rev. Lett.* **94**, 114801 (2005).
- M. Galletti, F. G. Bisesto, M. P. Anania, M. Ferrario, R. Pompili, A. Poyé, V. Tikhonchuk, and A. Zigler, *Appl. Phys. Lett.* **116**, 064102 (2020).
- V. Tikhonchuk, *Phys. Plasmas* **9**, 1416 (2002).
- Altechna, <https://www.altechna.com/products/windows/> (2020).
- M. Ferrario, D. Alesini, M. Anania, A. Bacci, M. Bellaveglia, O. Bogdanov, R. Boni, M. Castellano, E. Chiadroni, A. Cianchi *et al.*, *Nucl. Instrum. Meth. B* **309**, 183 (2013).
- F. Bisesto, M. Anania, M. Bellaveglia, E. Chiadroni, A. Cianchi, G. Costa, A. Curcio, D. Di Giovenale, G. Di Pirro, M. Ferrario *et al.*, *Nucl. Instrum. Meth. A* (2018).
- F. Bisesto, M. Galletti, M. P. Anania, M. Ferrario, R. Pompili, and other, *High Power Laser Sci. Eng.* **7** (2019).
- A. Curcio, M. Anania, F. Bisesto, M. Botton, M. Castellano, E. Chiadroni, A. Cianchi, M. Ferrario, M. Galletti, D. Giulietti *et al.*, *Phys. Rev. Appl.* **9**, 024004 (2018).
- F. Beg, A. Bell, A. Dangor, C. Danson, A. Fewes, M. Glinsky, B. Hammel, P. Lee, P. Norreys, and M. Tatarakis, *Phys. plasmas* **4**, 447 (1997).
- M. Haines, M. Wei, F. Beg, and R. Stephens, *Phys. Rev. Lett.* **102**, 045008 (2009).
- R. Town, C. Chen, L. Cottrill, M. Key, W. Krueer, A. Langdon, B. Lasinski, R. Snavely, C. Still *et al.*, *Nucl. Instrum. Meth. A* **544**, 61 (2005).
- A. Poyé, S. Hulin, M. Bailly-Grandvaux, J. Dubois, J. Ribolzi, D. Raffestin, M. Bardon, F. Lubrano-Lavaderci, E. D'Humières, J. J. Santos *et al.*, *Phys. Rev. E* **91**, 043106 (2015).
- X. Vaisseau, A. Debayle, J. J. Honrubia, S. Hulin, A. Morace *et al.*, *Phys. Rev. Lett.* **114**, 095004 (2015).
- H. Deng, K. J. Leedle, Y. Miao, D. S. Black, K. E. Urbanek, J. McNeur, M. Kozak, A. Ceballos, P. Hommelhoff, O. Solgaard, R. L. Byer, and J. S. Harris, *Adv. Opt. Mater.* **8**, 2070026 (2020).
- M. Kozak, P. Beck, H. Deng, J. McNeur, N. Schönerberger, C. Gaida, F. Stutzki, M. Gebhardt *et al.*, *Opt. Express* **25**, 19195 (2017).

## FULL REFERENCES

1. B. A. Remington, D. Arnett, R. Paul *et al.*, "Modeling astrophysical phenomena in the laboratory with intense lasers," *Science* **284**, 1488–1493 (1999).
2. T. Bartal, M. E. Foord, C. Bellei, M. H. Key, K. A. Flippo, S. A. Gaillard, D. T. Offermann, P. K. Patel *et al.*, "Focusing of short-pulse high-intensity laser-accelerated proton beams," *Nat. Phys.* **8**, 139–142 (2012).
3. D. Kaganovich, D. Gordon, and A. Ting, "Observation of large-angle quasimonoenergetic electrons from a laser wakefield," *Phys. Rev. Lett.* **100**, 215002 (2008).
4. M. Kozak, J. McNeur, K. Leedle *et al.*, "Optical gating and streaking of free electrons with sub-optical cycle precision," *Nat. Comm.* **8**, 14342 (2017).
5. J. McNeur, M. Kozak, N. Schönenberger, K. J. Leedle, H. Deng, A. Ceballos, H. Hoogland, A. Ruehl, I. Hartl, R. Holzwarth, O. Solgaard, J. S. Harris, R. L. Byer, and P. Hommelhoff, "Elements of a dielectric laser accelerator," *Optica*, **5**, 687–690 (2018).
6. K. W. Ledingham, P. R. Bolton, N. Shikazono, and C.-M. C. Ma, "Towards laser driven hadron cancer radiotherapy: A review of progress," *Appl. Sci.* **4**, 402–443 (2014).
7. E. Clark, K. Krushelnick, M. Zepf, F. Beg, M. Tatarakis, A. Machacek, M. Santala, I. Watts, P. Norreys, and A. Dangor, "Energetic heavy-ion and proton generation from ultraintense laser-plasma interactions with solids," *Phys. Rev. Lett.* **85**, 1654 (2000).
8. R. Snavely, M. Key, S. Hatchett, T. Cowan, M. Roth, T. Phillips, M. Stoyer, E. Henry, T. Sangster, M. Singh *et al.*, "Intense high-energy proton beams from petawatt-laser irradiation of solids," *Phys. Rev. Lett.* **85**, 2945 (2000).
9. A. Mackinnon, Y. Sentoku, P. Patel, D. Price, S. Hatchett, M. Key, C. Andersen, R. Snavely, and R. Freeman, "Enhancement of proton acceleration by hot-electron recirculation in thin foils irradiated by ultraintense laser pulses," *Phys. Rev. Lett.* **88**, 215006 (2002).
10. J. Dubois, F. Lubrano-Lavaderci, D. Raffestin, J. Ribolzi, J. Gazave, A. C. La Fontaine, E. d'Humières, S. Hulin, P. Nicolaï, A. Poyé *et al.*, "Target charging in short-pulse-laser-plasma experiments," *Phys. Rev. E* **89**, 013102 (2014).
11. A. Poyé, J. Dubois, F. Lubrano-Lavaderci, E. D'Humières, M. Bardou, S. Hulin, M. Bailly-Grandvaux, J. Ribolzi, D. Raffestin, J. Santos *et al.*, "Dynamic model of target charging by short laser pulse interactions," *Phys. Rev. E* **92**, 043107 (2015).
12. A. Macchi, M. Borghesi, and M. Passoni, "Ion acceleration by superintense laser-plasma interaction," *Rev. Mod. Phys.* **85**, 751 (2013).
13. S. Wilks, A. Langdon, T. Cowan, M. Roth, M. Singh, S. Hatchett, M. Key, D. Pennington, A. MacKinnon, and R. Snavely, "Energetic proton generation in ultra-intense laser-solid interactions," *Phys. Plasmas* **8**, 542–549 (2001).
14. O. Jäckel, J. Polz, S. Pfotenhauer, H. Schlenvoigt, H. Schwoerer, and M. Kaluza, "All-optical measurement of the hot electron sheath driving laser ion acceleration from thin foils," *New J. Phys.* **12**, 103027 (2010).
15. P. Nilson, J. Davies, W. Theobald, P. Jaanimagi, C. Mileham, R. Jungquist, C. Stoeckl, I. Begishev, A. Solodov, J. Myatt *et al.*, "Time-resolved measurements of hot-electron equilibration dynamics in high-intensity laser interactions with thin-foil solid targets," *Phys. Rev. Lett.* **108**, 085002 (2012).
16. J. T. Morrison, S. Feister, K. D. Fricke, D. R. Austin, G. K. Ngirmang, N. R. Murphy, C. Orban, E. A. Chowdhury, and W. Roquemore, "MeV proton acceleration at kHz repetition rate from ultra-intense laser liquid interaction," *New J. Phys.* **20**, 022001 (2018).
17. R. Pompili, M. Anania, F. Bisesto, M. Botton, M. Castellano, E. Chiadroni, A. Cianchi, A. Curcio, M. Ferrario, M. Galletti *et al.*, "Femtosecond dynamics of energetic electrons in high intensity laser-matter interactions," *Sci. Rep.* **6**, 35000 (2016).
18. R. Pompili, M. Anania, F. Bisesto, M. Botton, E. Chiadroni, A. Cianchi, A. Curcio, M. Ferrario, M. Galletti *et al.*, "Ultrafast evolution of electric fields from high-intensity laser-matter interactions," *Sci. Rep.* **8**, 3243 (2018).
19. R. Pompili, M. Anania, F. Bisesto, M. Botton, M. Castellano, E. Chiadroni, A. Cianchi, A. Curcio, M. Ferrario, M. Galletti *et al.*, "Sub-picosecond snapshots of fast electrons from high intensity laser-matter interactions," *Opt. Express* **24**, 29512–29520 (2016).
20. F. Bisesto, M. P. Anania, M. Botton, E. Chiadroni, A. Cianchi, A. Curcio, M. Ferrario, M. Galletti *et al.*, "Novel single-shot diagnostics for electrons from laser-plasma interaction at sparc\_lab," *Quantum Beam Sci.* **1**, 13 (2017).
21. F. Bisesto, M. Galletti, M. Anania, M. Ferrario, R. Pompili *et al.*, "Single-shot electrons and protons time-resolved detection from high-intensity laser-solid matter interactions at sparc\_lab," *High Power Laser Sci. Eng.* **7** (2019).
22. B. Steffen, V. Arsov, G. Berden, W. Gillespie, S. Jamison, A. M. MacLeod, A. Van Der Meer, P. Phillips, H. Schlarb, B. Schmidt *et al.*, "Electro-optic time profile monitors for femtosecond electron bunches at the soft x-ray free-electron laser flash," *Phys. Rev. Special Top. Beams* **12**, 032802 (2009).
23. A. L. Cavalieri, D. Fritz, S. Lee, P. Bucksbaum, D. Reis, J. Rudati, D. Mills, P. Fuoss, G. Stephenson, C. Kao *et al.*, "Clocking femtosecond x rays," *Phys. Rev. Lett.* **94**, 114801 (2005).
24. M. Galletti, F. G. Bisesto, M. P. Anania, M. Ferrario, R. Pompili, A. Poyé, V. Tikhonchuk, and A. Zigler, "Direct observation of ultrafast electrons generated by high-intensity laser-matter interaction," *Appl. Phys. Lett.* **116**, 064102 (2020).
25. V. Tikhonchuk, "Interaction of a beam of fast electrons with solids," *Phys. Plasmas* **9**, 1416–1421 (2002).
26. Altechna, <https://www.altechna.com/products/windows/> (2020).
27. M. Ferrario, D. Alesini, M. Anania, A. Bacci, M. Bellaveglia, O. Bogdanov, R. Boni, M. Castellano, E. Chiadroni, A. Cianchi *et al.*, "SPARC\_LAB present and future," *Nucl. Instrum. Meth. B* **309**, 183–188 (2013).
28. F. Bisesto, M. Anania, M. Bellaveglia, E. Chiadroni, A. Cianchi, G. Costa, A. Curcio, D. Di Giovenale, G. Di Pirro, M. Ferrario *et al.*, "The flame laser at sparc\_lab," *Nucl. Instrum. Meth. A* (2018).
29. F. Bisesto, M. Galletti, M. P. Anania, M. Ferrario, R. Pompili, and other, "Review on tnsa diagnostics and recent developments at sparc\_lab," *High Power Laser Sci. Eng.* **7** (2019).
30. A. Curcio, M. Anania, F. Bisesto, M. Botton, M. Castellano, E. Chiadroni, A. Cianchi, M. Ferrario, M. Galletti, D. Giulietti *et al.*, "Electro-optical detection of coherent radiation induced by relativistic electron bunches in the near and far fields," *Phys. Rev. Appl.* **9**, 024004 (2018).
31. F. Beg, A. Bell, A. Dangor, C. Danson, A. Fewes, M. Glinsky, B. Hammel, P. Lee, P. Norreys, and M. Tatarakis, "A study of picosecond laser-solid interactions up to  $10^{19} \text{ W} \cdot \text{cm}^{-2}$ ," *Phys. plasmas* **4**, 447–457 (1997).
32. M. Haines, M. Wei, F. Beg, and R. Stephens, "Hot-electron temperature and laser-light absorption in fast ignition," *Phys. Rev. Lett.* **102**, 045008 (2009).
33. R. Town, C. Chen, L. Cottrill, M. Key, W. Kruer, A. Langdon, B. Lasinski, R. Snavely, C. Still *et al.*, "Simulations of electron transport for fast ignition using lsp," *Nucl. Instrum. Meth. A* **544**, 61–66 (2005).
34. A. Poyé, S. Hulin, M. Bailly-Grandvaux, J. Dubois, J. Ribolzi, D. Raffestin, M. Bardou, F. Lubrano-Lavaderci, E. D'Humières, J. J. Santos *et al.*, "Physics of giant electromagnetic pulse generation in short-pulse laser experiments," *Phys. Rev. E* **91**, 043106 (2015).
35. X. Vaisseau, A. Debayle, J. J. Honrubia, S. Hulin, A. Morace *et al.*, "Enhanced relativistic-electron-beam energy loss in warm dense aluminum," *Phys. Rev. Lett.* **114**, 095004 (2015).
36. H. Deng, K. J. Leedle, Y. Miao, D. S. Black, K. E. Urbanek, J. McNeur, M. Kozak, A. Ceballos, P. Hommelhoff, O. Solgaard, R. L. Byer, and J. S. Harris, "Ga2o3-based optical applications: Gallium oxide for high-power optical applications (advanced optical materials 7/2020)," *Adv. Opt. Mater.* **8**, 2070026 (2020).
37. M. Kozak, P. Beck, H. Deng, J. McNeur, N. Schönenberger, C. Gaida, F. Stutzki, M. Gebhardt *et al.*, "Acceleration of sub-relativistic electrons with an evanescent optical wave at a planar interface," *Opt. Express* **25**, 19195–19204 (2017).